Journal of Porous Materials (2025) 32:2443–2453
https://doi.org/10.1007/s10934-025-01844-4

Eco-friendly synthesis of carbon nanomaterials from pumpkin waste

Scarlett Allende[1] · Yang Liu[2] · Muhammad Adeel Zafar[1] · Mohan V. Jacob[1]

Received: 17 June 2025 / Accepted: 25 July 2025 / Published online: 22 September 2025

Abstract

Waste management remains a major environmental challenge in the food sector, making the recovery and reuse of organic waste essential. This study presents a novel and optimised approach to converting pumpkin peel waste into high-quality carbon material using microwave-assisted pyrolysis (MAP), without the use of chemical additives or metal doping. The resulting carbon nanomaterial exhibits desirable characteristics, including crystalline to semicrystalline carbon nanoparticles (lattice spacing of 2.29 Å), microporosity of 29.1 m²/g, and a pore diameter of 3.7 nm, along with enhanced electron transfer kinetics (Rct = 563 Ω). This carbon material was employed to modify a screen-printed carbon electrode (SPCE) for the electrochemical detection of nitrite. The modified electrode shows a significant improvement in electrochemical response, with an increase in current output from 20 µA to 30 µA, resulting in higher conductivity, a broader Linear detection range, and a lower detection Limit of 10 µM. This work demonstrates a promising result for upcycling food waste into functional nanomaterials, offering both environmental benefits and practical applications in electrochemical sensing technologies.

Graphical abstract

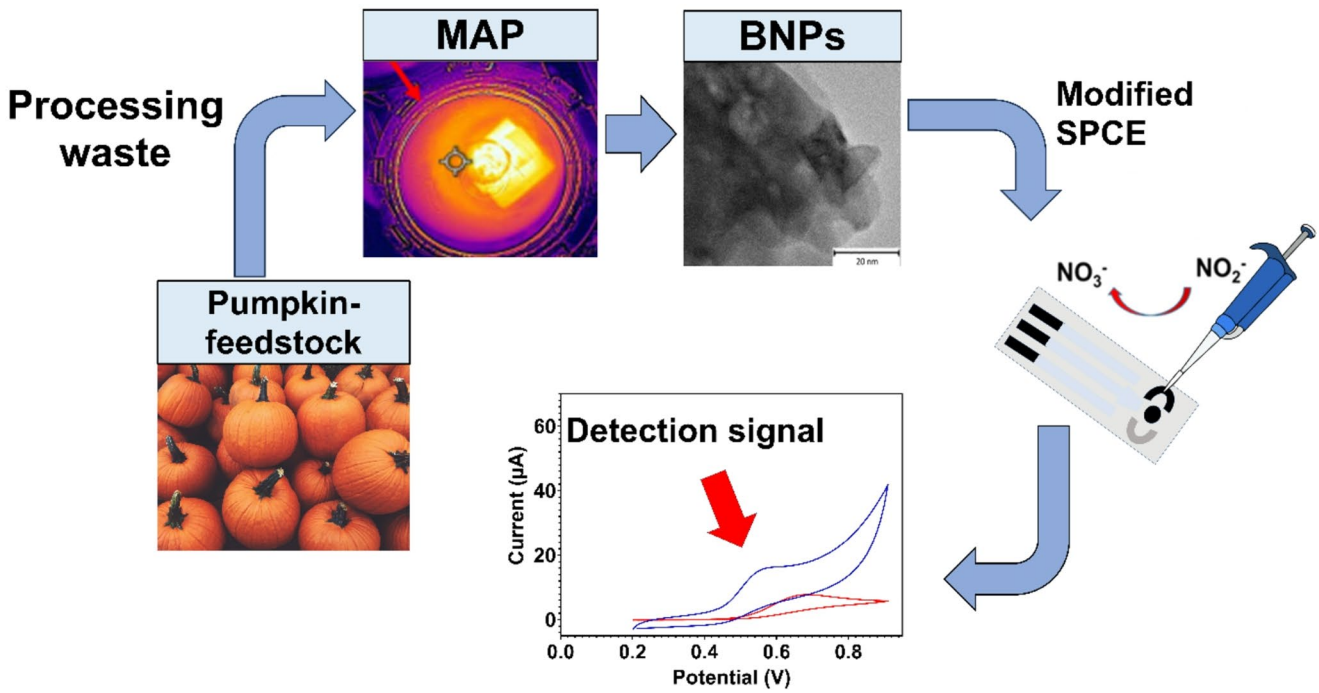

Keywords Biochar · Microwave-assisted pyrolysis · Screen-printed carbon electrode · Nitrite

Extended author information available on the last page of the article

1 Introduction

The disposal of food waste has become a critical environmental concern due to the large food demand (1.3 bn t per year), lack of space for dumping residues, and the release of greenhouse gas emissions. The challenges in the food processing industry are associated with excessive consumption of non-renewable sources (water), considerable environmental waste impact (8% global greenhouse gas emissions), and economic cost [1–3]. The assessment of food waste generation per capita in Europe and North America is 95–115 kg/year [4]. Particularly, for the period 2016, the world's pumpkin production is estimated at 26.49 MMT [5]. Therefore, recovering industrial waste into carbon-rich materials using an efficient conversion method offers a sustainable solution for waste management.

Agricultural waste management encompasses various scenarios, including burning, composting, animal feeding, and landfill disposal [6, 7]. Other types of biomass treatment rely on biochemical and chemical processing methods, such as anaerobic digestion, fermentation, and conventional and microwave pyrolysis. MAP offers a higher heating efficiency, which is beneficial for breaking down waste in a shorter reaction time [8, 9]. MAP technology is an electromagnetic heating method in which heat energy is transferred through the interaction of molecules inside the feedstock material to the external surface (heat generated from within the biomass) in an oxygen-free environment [8, 10, 11].

The inappropriate management of certain inorganic species, such as nitrite, poses serious environmental and health risks due to their presence in contaminated water, food, and soil. Nitrite is a hazardous molecule known for its carcinogenic potential in humans and its toxic effects on aquatic life [12, 13]. Given its widespread occurrence and harmful nature, nitrite was selected as the target analyte to demonstrate the sensing capability of the developed biochar material. To assess the anti-interference ability of the BNPs/SPCE sensor, common interferents such as nitrate, chloride, and sulphate were tested at concentrations of 0.5 mM, providing a realistic and stringent evaluation. This study highlights the potential of using food residues, such as pumpkin peel, as a sustainable feedstock for producing porous carbon materials via microwave-assisted pyrolysis (MAP), offering an eco-friendly approach for fabricating electrochemical sensors for harmful inorganic species [14, 15].

Most carbon materials employed in modified electrodes for sensing applications typically involve complex synthesis processes, such as biomass pre- or post-treatment and the use of non-sustainable additives like metals. These approaches raise concerns about environmental impact, cost, and scalability [12, 16–18]. Therefore, there is an urgent need in the technological sector for the synthesis of sustainable and high-quality biomass-derived carbon materials [19, 20]. In response, this work studies a sustainable and simplified fabrication approach using MAP to convert untreated biomass into carbon nanomaterials. This simplified process eliminates the need for harsh chemicals or metal doping while preserving desirable structural and electrochemical properties. The resulting material exhibits strong potential for sensitive and selective detection of nitrite, highlighting its relevance for practical and eco-friendly sensor applications.

2 Experimental

2.1 Preparation of carbon nanomaterial

The raw pumpkin peel was thoroughly washed with distilled water and dried in an oven at 110 °C for 2 h. The dried biomass was then subjected to microwave-assisted pyrolysis (MAP) at 1.2 kW for 30 min under a nitrogen atmosphere, using 10% (w/w) of a microwave susceptor. The resulting biochar was further dried in an oven at 110 °C for 1 h. The selection of these MAP parameters was based on the optimisation of operating conditions, evaluating three microwave power settings—0.9 kW, 1.2 kW, and 1.5 kW—for a fixed duration of 40 min. Detailed results of this optimisation are reported in [1].

The metal-free carbon nanomaterial was obtained without pre- or post-chemical treatment. Activated carbon was selected as a microwave due to its high dielectric properties (~0.9 tanδ), providing better pyrolysis heating rates in the breakdown of feedstock than biochar (~0.2 tanδ) [8]. The MAP system used in the experimental work is shown in Fig. 1. The system is composed of (a) carrier gas (N_2, 4 L/min), (b) a chamber where the pyrolysis occurs, (c) an auto-tuner for controlling the reflected power, (d) 3 kW microwave generator, (e) a microwave controller, (f) condenser setting, and (g) vacuum pump.

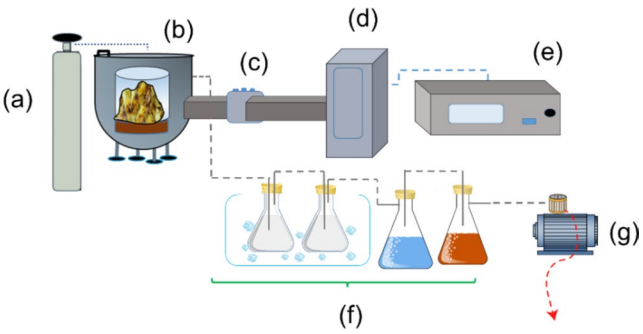

Fig. 1 Microwave pyrolysis system used in the production of BNPs, which components are: **a** N_2 carrier gas; **b** custom-made chamber; **c** auto-tuner; **d** 3 kW microwave generator; **e** controller; **f** flask condensers and **g** vacuum pump

2.2 Electrode Preparation for electrochemical study

The biochar was first ground into a fine powder using a mortar and pestle to achieve a uniform particle size suitable for electrode modification. The carbon material was then dispersed in ethanol and subjected to ultrasonication for one hour to ensure homogenous suspension, leveraging ethanol's excellent dispersibility with carbon-based nanomaterials [21]. The resulting dispersion exhibited good short-term stability and was used immediately after sonication to ensure consistent coating performance [21, 22]. A drop-casting technique was employed by depositing 1 µL of a 1 mg mL^{-1} dispersion onto the surface of a screen-printed carbon electrode (SPCE), followed by air drying at room temperature. This method was selected based on the porous and partially graphitic structure of the biochar, which facilitates uniform distribution and effective surface adhesion, as supported by prior studies [23, 24], confirming its suitability for electrochemical applications (Fig. 2).

2.3 Reagents and instruments

Sodium nitrite ($NaNO_2$) was purchased from Sigma-Aldrich. The PBS solution (phosphate-buffered solution, pH 7.0) was prepared using a solution based on dibasic-Na_2HPO_4 and monobasic-NaH_2PO_4. The electrochemical experiments were performed using a PalmSens4 potentiostat (PalmSens, Netherlands). The SPCEs (dimension 0.8 × 4.5 cm) were purchased from PalmSens, which comprises a silver pseudo reference electrode, a circular carbon working electrode (thickness: 200 µm) and a graphite counter electrode. The geometric area of the bare working electrode and BNPs/SPCE is 7.07 mm^2 and 7.09 mm^2, respectively. The BNPs were characterised by using the following techniques: Transmission Electron Microscopy (TEM) imaging using JEOL 2100 TEM; surface area measured by Micromeritics 3-flex surface and porosity analyser; Scanning Electron Microscopy (SEM) images obtained using JEOL 7001 F SEM; Fourier transform infrared spectra (FTIR) were performed using Nicolet iS50 FT-IR Spectrometer; and Raman spectrum by Renishaw In-Via Micro-Raman spectrometer.

3 Results and discussion

3.1 Characterisation of BNPs

The ultimate analysis of pumpkin peel biochar is shown in Table 1. Minor carbon concentration was observed (41.76%) in BNPs with a high presence of oxygen (17.87%) and sulphur (19.37%) content. The performance is associated with the treatment time (30 min), a short reaction time was not enough to fully breakdown organic chemical bonds (high inorganic compounds), like C—H and C—O, reducing the carbon formation [10]. This information is correlated with the TEM/EDS studied in the following results section. However, high microwave power led to high heating rates, which promotes the rapid formation of volatile matter, generating small pores but high pore volume [8, 10]. This finding is supported by SEM imaging. In the thermochemical process, Nanopores with an average adsorption pore diameter of 3.7 nm and a pore volume of 0.13 cm3/g were formed. A pore volume of 0.13 cm^3/g further supports the formation of porous networks suitable for electrochemical applications [10, 24, 25].

SEM images of BNPs are shown in Fig. 3 (a1) and (a2). The material surface reveals deep cavities and small and irregular microporous morphology. This finding is associated with the high microwave power treatment, which generates microporosity, irregular surface and structural damage to the biochar [1, 10]. Figure 3 (a2) also shows some block pores zones, which are associated with unpyrolyzed organic matter and mineral ash [26]. TEM images denote that the organic mix is a crystalline to semi-crystalline structure. Figure 3 (b1) illustrates the bubbling effect from beam damage to the area, which is linked to the presence of O, P, K,

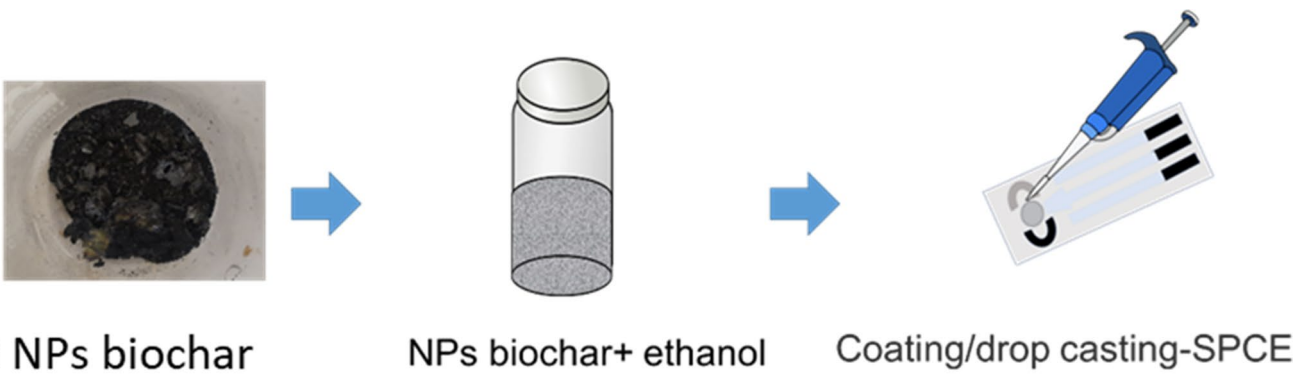

Fig. 2 Fabrication scheme of BNPs/SPCE

Table 1 CHNSO elemental analysis and surface area data of BNPs

Elements (%)	
C	41.76
H	4.62
N	16. 38
S	19.37
O	17.87
Surface area	
BET surface area (m^2/g)	89.98
t-Plot external area (m^2/g)	60.88
Pore volume < 628.1428 nm diameter (cm^3/g)	0.083
t-Plot micropore area (m^2/g)	29.1
t-Plot micropore volume (cm^3/g)	0.13
Average adsorption pore diameter nm (4 V/A)	3.7

and Ca. As EDS shows, high organic blends were detected on the base matrix, and some carbon was included. Some sheets were observed rolled into a tube-like structure relative to a high concentration of species like O, P, K, and Ca and minor Cu presence. A slightly stable crystallinity presence in some regions was achieved due to the existence of Mg, and multilayers are observed in Fig. 3 (b2). The carbon interacting with the large Fe particle has formed a ribbon around the particle, with layers of order/organisation into lattice planes. Figure 3 (d2) shows a lattice spacing of 2.29 Å obtained from degrading areas that roughly overlay Ca, P, O, and a minor concentration of Mg, Si, and Cu.

The functional groups on the surface of pumpkin peel biochar were studied using FTIR spectra analysis, as shown in Fig. 4. The bending vibration of hydroxyl functional groups (—OH) with considerably broad absorption bands was detected at 2750–3200 cm^{-1}. A minor presence of aliphatic groups was detected at 2600 cm^{-1}. The peak at 1450 cm^{-1} corresponds to aromatic functional groups C = O, e.g., carbonyl oxygen-containing groups. Stretching vibration of C—O—C was observed at 1490 cm^{-1} [27–29]. Figure 4 (b) shows the RAMAN curve of BNPs. The D band specifies the presence of structural defects of carbon domains within the biochar nanoparticles, as shown [30]. G band denotes the presence of graphitic or crystalline carbon structures in the BNPs, and G′ suggests partial graphitisation or multilayer graphene-like stacking in the biochar. D + G band indicates mixed structural domains. Similar results are reported in [23, 25].

3.2 Electrochemical characterisation

The interfacial charge transfer properties of the modified SPCEs were evaluated using electrochemical impedance spectra (EIS), shown in Fig. 5 (a). The diameter of the semicircle represents the electron charge transfer resistance (R_{ct}) characteristic of the SCPE surface. A pseudo-linear region

Fig. 3 SEM (**a1**) (**a2**), TEM (**b1**) (**b2**), EDS (**c1**) (**c2**) and lattice spacing images (**d1**) (**d2**) of BNPs

denotes a diffusion process at a low-frequency range [24, 31]. The Nyquist plot demonstrates that BNPs/SPCE shows higher electron transfer kinetic properties than bare SPC electrodes and, therefore, higher conductivity. This electrochemical behaviour is attributed to the reactive oxygen-containing functional groups on the BNP surface, along with its high surface area (29.1 m^2/g), nanoscale porosity (3.7 nm), and abundant active sites. These features facilitate faster electron transfer and enhanced analyte interaction [24, 25]. The semicrystalline structure and defect sites further support conductivity and electrocatalytic performance, as confirmed by Raman and TEM analyses. The circuit diagram is described in the Nyquist plot, which comprises the electrolyte resistance (R_1), charge transfer resistance property (R_2), double layer capacitance (Cdl) and Warburg impedance (W). The Rct of bare SPCE and BNPs/SPCE was found to be 10kΩ and 563Ω, respectively. The cyclic voltammetry (CV) shows that the BNPs/SPCE achieved a higher redox current response (30 µA vs. 20 µA) and smaller peak-to-peak separation than the bare electrode, indicating that the BNPs increased the electroactive area. Based on the CV results shown in Fig. 5 (b), the effective area of bare and modified electrodes was calculated as 0.077cm^2 and 0.118cm^2, respectively by using Randles–Sevcik equation ($I_p = (2.69 \cdot 10^5)\, n^{3/2}\, A\, D_0^{1/2}\, v^{1/2}\, c_0$), where I_p is the maximum current (µA), n is the number of electrons participating in the redox reaction (e.g. equal 1), A is the effective area of the electrode (cm^2), D_0 is the diffusion coefficient 7.6×10^{-6} cm^2/s for $K_3[Fe(CN)_6]$, v is the potential scan rate (V/s), c_0 is the concentration of the redox probe (5 mM $K_3[Fe(CN)_6]$).

3.3 Electrochemical detection of nitrite

The electrocatalytic properties of bare and modified electrodes for detecting nitrite were investigated using the CV technique. Figure 6 shows the CV curves of different electrodes (bare SPCE and BNPs/SPCE) in blank PBS, and PBS containing nitrite. In the absence of nitrite, both electrodes showed only background current with no observable oxidation peaks (black and green curves), indicating no electrochemical activity in the base electrolyte. On the other hand, a prominent oxidation current signal was observed for BNPs/SPCE in PBS containing 0.5 mM nitrite at 0.56 V (blue curve), which is significantly lower than the oxidation potential of the bare SPCE (0.66 V), indicating improved catalytic activity. This enhancement is attributed to the biochar's porous architecture and rich surface chemistry—particularly oxygen-containing functional groups—which facilitate effective analyte adsorption, electron transfer, and diffusion pathways. Moreover, the presence of semi-crystalline graphitic domains in BNPs, as confirmed by Raman

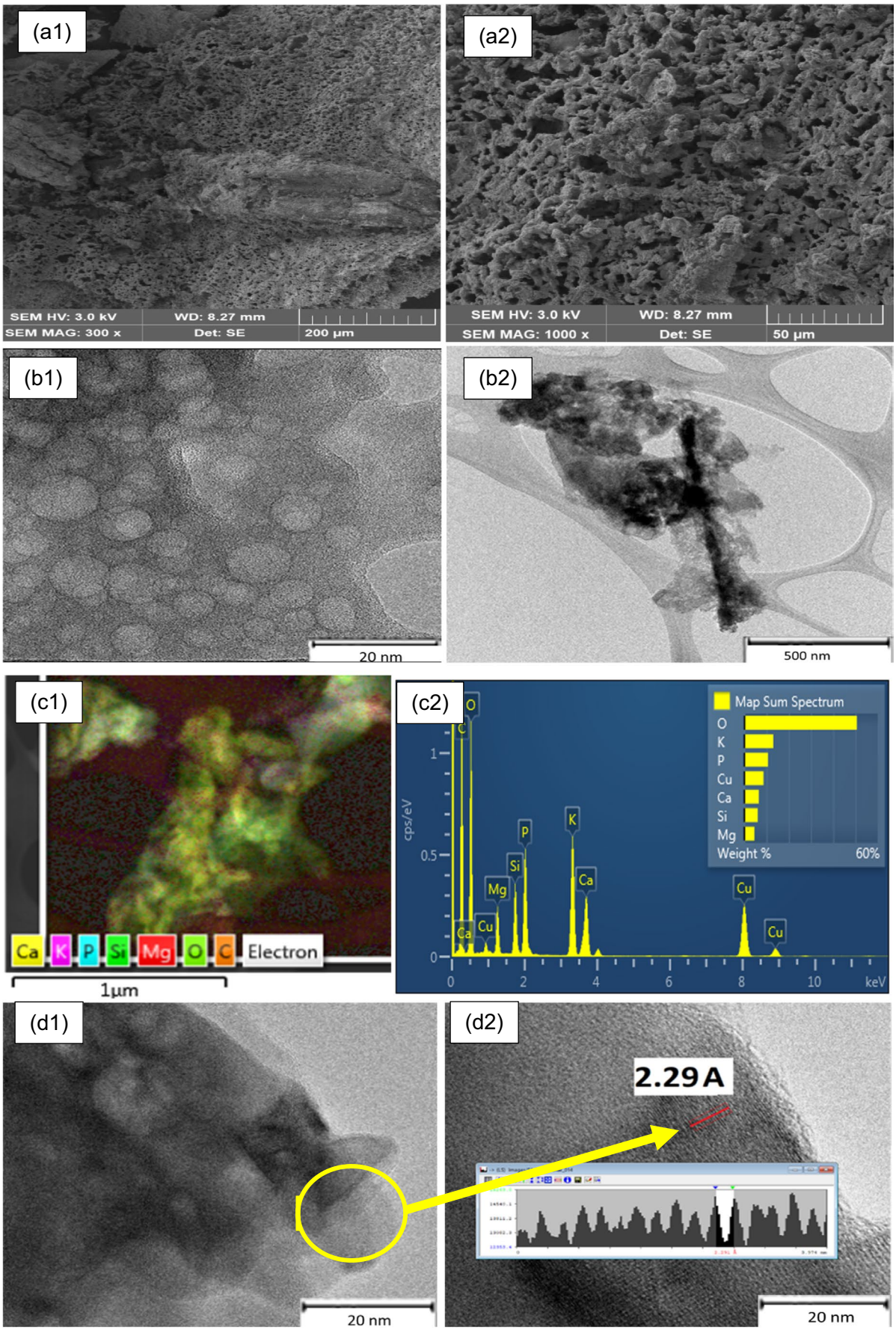
(a1)
SEM HV: 3.0 kV
WD: 8.27 mm
SEM MAG: 300 x
Det: SE
200 µm
(a2)
SEM HV: 3.0 kV
WD: 8.27 mm
SEM MAG: 1000 x
Det: SE
50 µm
(b1)
20 nm
(b2)
500 nm
(c1)
Ca K P Si Mg O C Electron
1µm
(c2)
Map Sum Spectrum
O
K
P
Cu
Ca
Si
Mg
Weight %
60%
cps/eV
keV
(d1)
20 nm
(d2)
2.29 A
20 nm

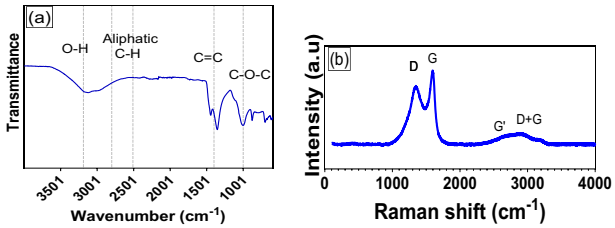

Fig. 4 **a** FTIR and **b** RAMAN curves of BNPs

and TEM analyses, likely promotes higher conductivity and rapid charge transport at the electrode interface, leading to enhanced electrocatalytic response [23, 24].

We employed differential pulse voltammetry (DPV) to investigate the linear range and the sensitivity of the MF NPs/SPCE electrode for 0.4–1.9 mM nitrite. For this purpose, nitrite was successively added to the 0.1 M PBS solution. DPV was selected over other techniques for the linear range analysis due to its low capacitive current and high sensitivity to detect oxidation peaks using minimum nitrite concentrations, helping to reduce the background charging currents, also the use of this technique provides consistency and data comparability with previous studies with similar carbon material properties for nitrite sensing reported in the literature as [32–35]. The limit of detection (LOD) was calculated considering the equation $LOD = 3S_b/m$, where S_b is the standard deviation in a blank solution (four measurements) and m is the slope of the correlation graph [36]. As shown in Fig. 7 (a), the oxidation peak current increased with the increase of nitrite concentration in the solution. The plot between peak currents and concentrations, along with

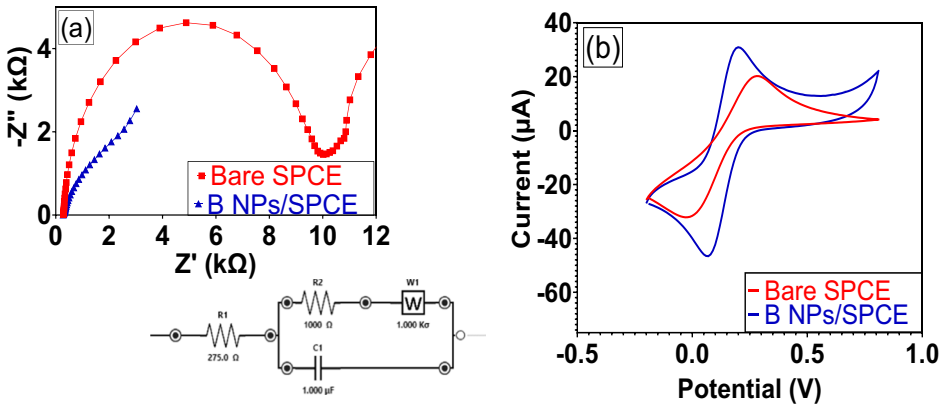

Fig. 5 EIS **a** and CV **b** curves of bare SPCE and BNPs/SPCE in 0.1 M KCl containing 5 mM $K_3[(Fe(CN)_6)]$ at a scan rate of 5 mV/s

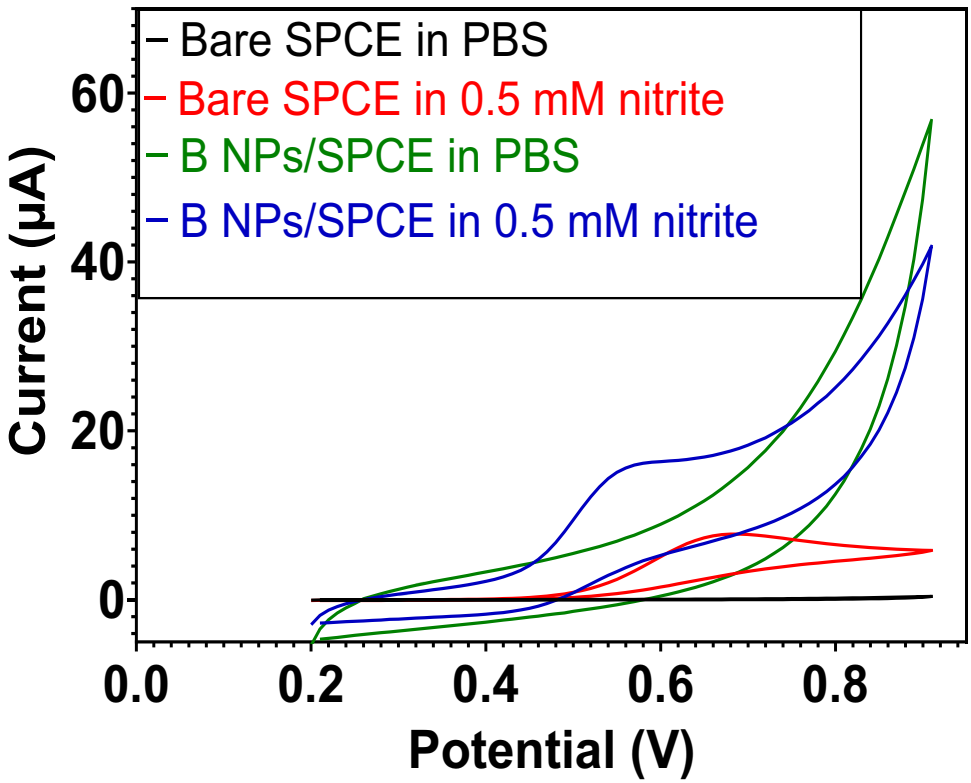

Fig. 6 CV curves of bare SPCE and modified SPCE in 0.1 M PBS solution and 0.5 mM nitrite at 0.05 V/s scan rate

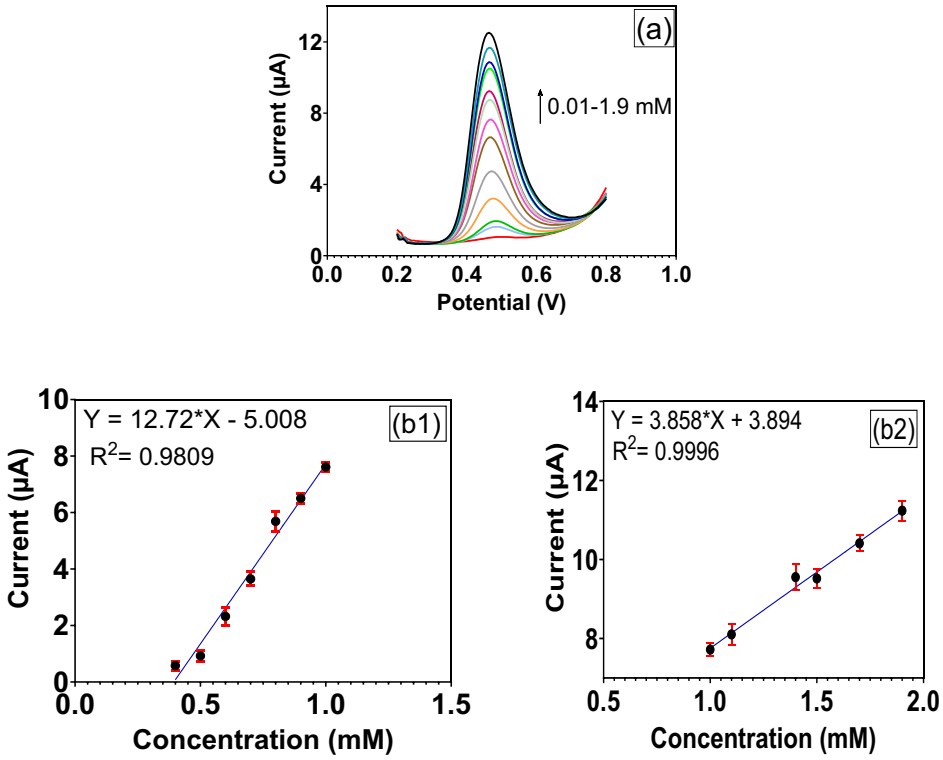

Fig. 7 DPVs (**a**) of BNPs/SPCE in 0.1 M PBS (pH 7.0) in the presence of various nitrite concentrations ranging from 0.01 to 1.9 mM. Calibration curve for low (0.4-1 mM) (**b1**) and high (1-1.9 mM) (**b2**) nitrite concentration against current response

calibration curves, is shown in Figs. 7 (b1) and (b2). The peak currents showed Linearity between 0.01 and 1.9 mM concentration of nitrite. The linear regression equations and the values of R^2 are given in the inset of Figs. 7 (b1) and (b2). From calibration equations is possible to observe a drop in sensitivity (from lower concentration to higher concentration), this is because at high concentrations, surface saturation effects and mass transport Limitations reduce the effective interaction between the analyte and the electrode, decreasing its sensitivity. The electrode showed a competitive LOD of 10 µM. Table 2 compares our findings with previous work reported in the literature. Our MF NPs/SPCE electrode showed a wider linear range than other proposed electrodes, where more than one base material (composites) was used to modify the electrode. Whereas we used synthesised biochar to modify the electrode. Our approach has the advantage of lower cost and avoids the time needed to make the composite.

Table 2 Comparison of the analytical performance of the proposed sensor with the past works

Electrode	Detection method	LOD (µM)	Linear range (µM)	Reference
RGO-MWCNTs/GCE	DPV	25	75-6060	[32]
GR/CD/SPCE	Amperometry	0.26	0.07–2150	[37]
CDP/GS/MWCNTs	DPV	1.65	5-6750	[35]
PEDOT-Gr/Ta	DPV	7	20–2000	[33]
CTAB-GO/MWCNT/GCE	DPV	1.5	5-800	[34]
ABC-800/GCE	Chronoamperometry	2.7	4.9–1184	[38]
$ZnCl_2$-activated biochar/GCE	Chronoamperometry	0.97	100–1400	[24]
BNPs/SPCE	DPV	10	10-1900	This work

3.4 Selectivity, stability, and reproducibility of bnps/spc electrode

To evaluate the selectivity of the BNPs/SPCE electrode for nitrite, common potential interfering compounds such as potassium chloride (KCl), potassium nitrate (KNO_3), calcium chloride ($CaCl_2$), glucose, potassium bromide (KBr) and urea were tested. The selection criteria for the analytes were based on a previous study reported in the literature [12, 38, 39], which is suitable for studying the typical common interfering ions. As shown in Fig. 8, a distinct and sharp current response was observed exclusively for nitrite, with no significant peaks recorded for the other tested species. This demonstrates the high selectivity of the BNPs/SPCE, which can be attributed to the presence of oxygenated functional groups, microporous structure, and high surface area of the biochar material, all of which facilitate preferential interaction and electrocatalytic oxidation of nitrite. These surface features enhance electron transfer kinetics and suppress nonspecific adsorption,

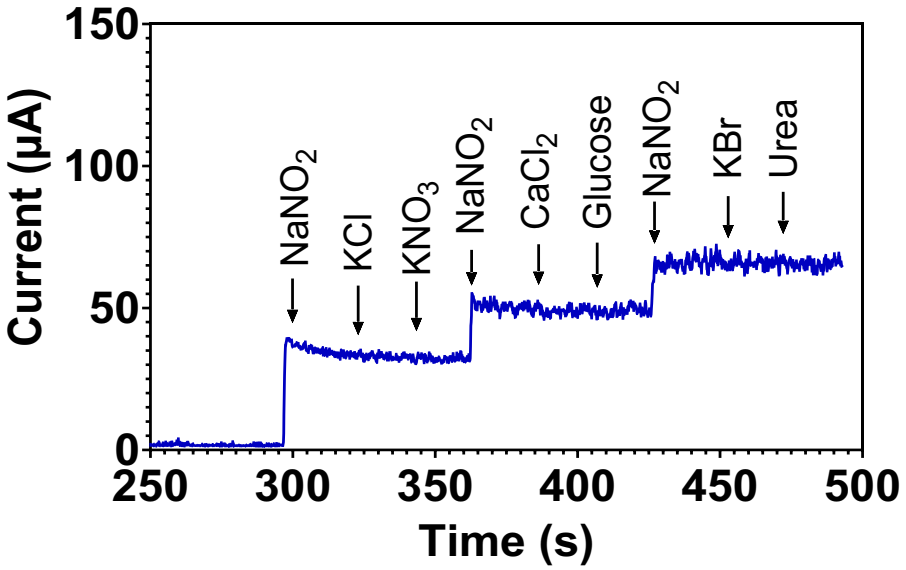

Fig. 8 Chronoamperometry response of BNPs/SPC electrode towards the addition of 0.5 mM nitrite and individual interfering species in 0.1 M PBS (pH 7.0)

enabling accurate detection even in the presence of electroactive species with similar functionalities.

To assess the reproducibility of the BNPs/SPCE electrode for the detection of nitrite by using the DPV technique, five parallel electrodes were employed. The electrodes showed admirable outcomes (up to 6 µA) with a relevant standard deviation (RSD) of 2.28%. The bar graph, indicating peak current values, is given in Fig. 9 (a). The stability of the electrode was also investigated. For this purpose, the electrode was stored for up to four days in an enclosed container and was investigated at the end of each day. The results in Fig. 9 (b) show that there were no significant changes in the oxidation current of the electrodes, and the RSD was 2.39%. This stability was repeated after 16 days of the first test (day $20^{th,}$ no consecutive). This value indicates excellent stability of the BNPs/SPCE electrode.

3.5 Real sample analysis

The feasibility of the BNPs/SPCE was validated through nitrite recovery in a real river water sample, as shown in Fig. 10. Using the standard addition method, 0.9 mM of nitrite was introduced into the sample, and the resulting current response was compared to that in PBS. A distinct oxidation peak was observed at 6.114 µA upon nitrite addition, while no peak was detected in the blank river water, indicating successful detection. The sensor achieved a recovery rate of 95%, confirming its applicability beyond laboratory conditions. A slight shift in oxidation potential from 0.50 V (PBS) to 0.49 V (river water) was noted, likely due to the lower pH of the river sample [40].

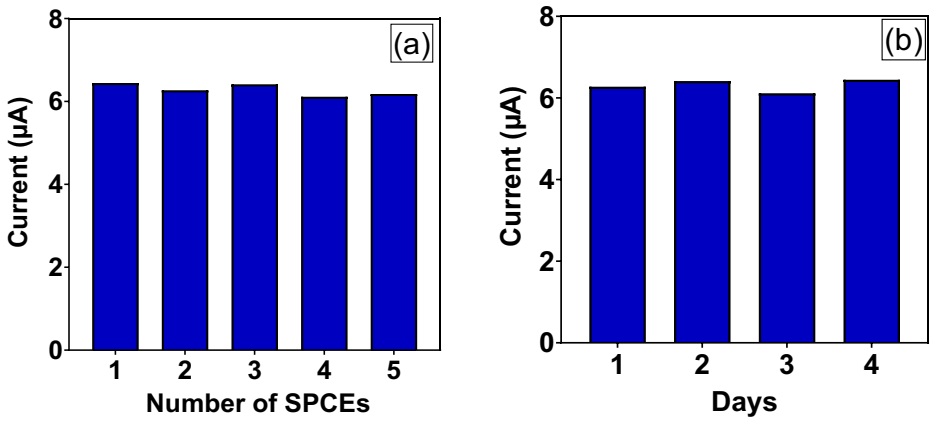

Fig. 9 Reproducibility a and stability b analysis of BNPs/SPCE in the presence of 0.5 mM nitrite in 0.1 M PBS (pH 7.0)

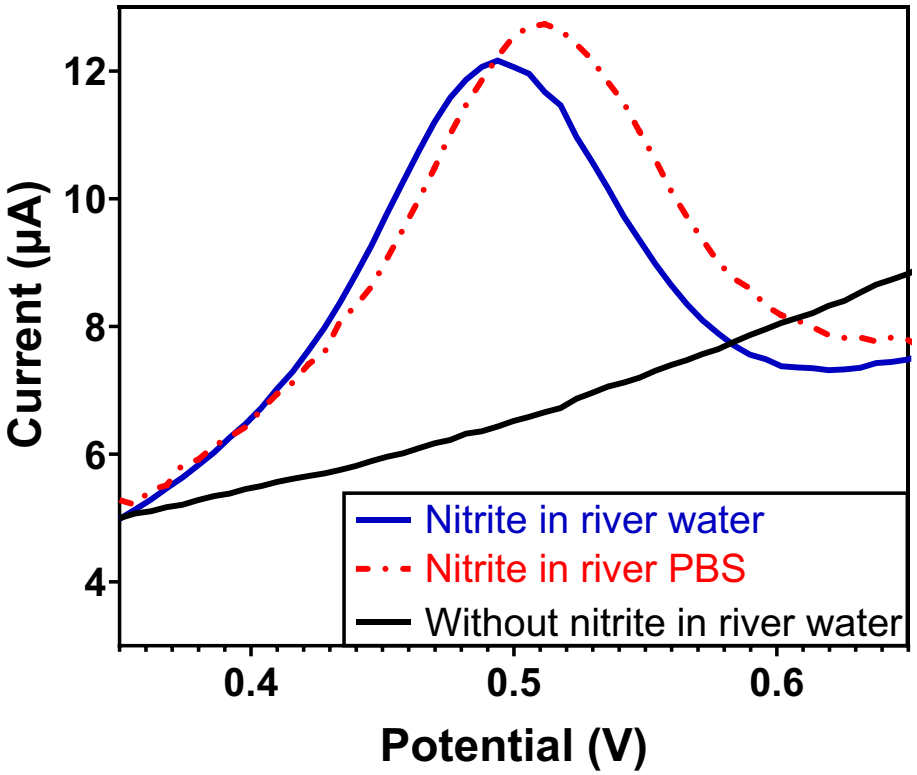

Fig. 10 DPV curves of BNPs/SPCE in 0.1 M PBS (pH 7.01) and river water (pH 6.92) containing 0.9 mM nitrite

4 Conclusion

This study demonstrates the successful synthesis of crystalline biochar nanoparticles from pumpkin peel waste using a rapid, low-cost, and chemical-free MAP process. The approach eliminates the need for harsh chemical treatments or expensive metal additives, making it both environmentally and economically viable. The resulting biochar exhibits a well-defined crystalline structure, enriched with oxygen-containing functional groups, and displays excellent physicochemical and electrocatalytic properties. These properties significantly enhance the performance of the BNPs/SPCE, particularly in terms of electron transfer kinetics, leading to improved electrochemical conductivity. The modified electrode showed promising performance for nitrite sensing, with a detection Limit of 10 μM, a recovery rate of 95%, and strong selectivity, stability, and reproducibility. This research highlights a sustainable alternative for valorising agricultural waste into functional carbon nanomaterials for electrochemical applications. The favourable electrocatalytic behaviour of the synthesised BNPs suggests potential use in sensing other environmental and biological analytes, contributing to both green materials development and advanced sensing technologies.

Acknowledgements The authors are grateful for the financial support of the Cooperative Research Centre for Developing Northern Australia and the support of its investment partners: the Western Australian, Northern Territory and Queensland Governments. S.A. also acknowledges the financial support of the James Cook University Postgraduate Research Scholarship.

Author contributions SA performed the methodology, formal analysis, writing of the original draft, and visualisation. YL supervision and data validation. MAZ completed the data validation, editing, and supervision. MVJ was a major contributor in the conceptualisation, writing, review & editing, supervision, and project administration. All authors read and approved the final manuscript.

Funding Open Access funding enabled and organized by CAUL and its Member Institutions.

Data availability No datasets were generated or analysed during the current study.

Declarations

Competing interests The authors declare no competing interests.

References

1. S. Allende et al., Energy recovery from pumpkin peel using microwave-assisted pyrolysis. Energies **16**, 6438 (2023b)
2. M. Chouaibi et al., Production of bioethanol from pumpkin peel wastes: comparison between response surface methodology (RSM) and artificial neural networks (ANN). Ind. Crops Prod. **155**, 112822 (2020)
3. R.B. Mansour et al., Improved recovery of antioxidant compounds from refined pumpkin peel extract: a mixture design method approach. Horticulturae **9**, 1111 (2023)
4. H.K. Jeswani et al., The extent of food waste generation in the UK and its environmental impacts. Sustain. Prod. Consum. **26**, 532–547 (2021)
5. C. Lalnunthari et al., Valorisation of pumpkin seeds and peels into biodegradable packaging films. Food Bioprod. Process. **118**, 58–66 (2019)
6. P. Duarah et al., A review on global perspectives of sustainable development in bioenergy generation. Bioresour. Technol. **348**, 126791 (2022)
7. B. Koul et al., Agricultural waste management strategies for environmental sustainability. Environ. Res. **206**, 112285 (2022)
8. S. Allende et al., Breakdown of biomass for energy applications using microwave pyrolysis: a technological review. Environ. Res. **226**, 115619 (2023a)
9. X. Li et al., Microwave pyrolysis coupled with conventional pre-pyrolysis of the stalk for syngas and biochar. Bioresour. Technol. **348**, 126745 (2022a)
10. S. Allende et al., Energy recovery from sugarcane bagasse under varying microwave-assisted pyrolysis conditions. Bioresour. Technol. Rep. **20**, 101283 (2022)
11. V. Hadiya et al., Biochar production with amelioration of microwave-assisted pyrolysis: current scenario, drawbacks and perspectives. Bioresour. Technol. **355**, 127303 (2022)
12. L. Cao et al., Rapid pyrolysis of Cu2+-polluted eggshell membrane into a functional Cu2+-Cu+/biochar for ultrasensitive electrochemical detection of nitrite in water. Sci. Total Environ. **723**, 138008 (2020)
13. R. Madhu et al., Heteroatom-enriched and renewable banana-stem-derived porous carbon for the electrochemical determination of nitrite in various water samples. Sci. Rep. **4**, 4679 (2014)
14. B.M. Matsagar, K.C.W. Wu, Chap. 1 - Agricultural waste-derived Biochar for environmental management, in Biochar in Agriculture for Achieving Sustainable Development Goals, ed. by D.C.W. Tsang, Y.S. Ok (Academic, 2022), pp. 3–13
15. R.S. Varma, Biomass-derived renewable carbonaceous materials for sustainable chemical and environmental applications. ACS Sustain. Chem. Eng. **7**, 6458–6470 (2019)
16. H. Cheng et al., Au-Pt@Biomass porous carbon composite modified electrode for sensitive electrochemical detection of Baicalein. Microchem. J. **154**, 104602 (2020)
17. Y. Li et al., Recent advances of biochar-based electrochemical sensors and biosensors. Biosensors (2022). https://doi.org/10.3390/bios12060377
18. D. Spanu et al., Biochar as an alternative sustainable platform for sensing applications: a review. Microchem. J. (2020). https://doi.org/10.1016/j.microc.2020.105506
19. M. Akilarasan et al., Synthesis of pyrochlore-type La2Sn2O7@GO for the in-situ profiling of organophosphate pesticides paraoxon ethyl in environmental samples. J. Environ. Chem. Eng. **12**, 111928 (2024)
20. D.R. Lobato-Peralta et al., Evaluating the impact of pre-carbonization on activated carbon production from animal-origin precursors for supercapacitor electrode applications. Biomass Bioenerg. **193**, 107574 (2025)
21. A. Martis et al., Production of graphene stably dispersible in ethanol by microwave reaction. Colloids Interfaces. **6**, 75 (2022)
22. D.W. Johnson et al., A manufacturing perspective on graphene dispersions. Curr. Opin. Colloid Interface Sci. **20**, 367–382 (2015)
23. S. Allende et al., Electrochemical sensing of paracetamol based on sugarcane bagasse-activated biochar. Ind. Crops Prod. **211**, 118241 (2024a)
24. S. Allende et al., Nitrite sensor using activated biochar synthesised by microwave-assisted pyrolysis. Waste Dispos. Sustain. Energy **5**, 1–11 (2023c)
25. S. Allende et al., Synthesis and application of biomass-based graphene oxide using microwave-assisted pyrolysis method. Nano-Structures & Nano-Objects **40**, 101338 (2024)
26. B. Bushra, N. Remya, Biochar from pyrolysis of rice husk biomass—characteristics, modification and environmental application. Biomass Convers. Biorefin. **14**, 5759–5770 (2024)
27. H. Nan et al., Interaction of inherent minerals with carbon during biomass pyrolysis weakens biochar carbon sequestration potential. ACS Sustainable Chem. Eng. **7**, 1591–1599 (2019)
28. M. Wu et al., Rice (*Oryza sativa* L) plantation affects the stability of biochar in paddy soil. Sci. Rep. **5**, 10001 (2015)
29. W. Xu et al., Bioavailability and speciation of cadmium in contaminated paddy soil as alleviated by biochar from co-pyrolysis of peanut shells and maize straw. Environ. Sci. Eur. **34**, 69 (2022)
30. S.S. Hegde et al., A novel and ultrasensitive high-surface porous carbon-based electrochemical biosensor for early detection of dengue virus. Biosens. Bioelectronics: X. **20**, 100525 (2024)
31. H.S. Magar et al., Electrochemical impedance spectroscopy (EIS): principles, construction, and biosensing applications. Sensors. **21**, 6578 (2021)
32. F. Hu et al., Study on the application of reduced graphene oxide and multiwall carbon nanotubes hybrid materials for simultaneous determination of catechol, hydroquinone, p-cresol and nitrite. Anal. Chim. Acta **724**, 40–46 (2012)
33. F. Tian et al., Synthesis of one-dimensional poly(3,4-ethylenedioxythiophene)-graphene composites for the simultaneous detection of hydroquinone, catechol, resorcinol, and nitrite. Synth. Met. **226**, 148–156 (2017)
34. Y.J. Yang, W. Li, CTAB functionalized graphene oxide/multiwalled carbon nanotube composite modified electrode for the simultaneous determination of ascorbic acid, dopamine, uric acid and nitrite. Biosens. Bioelectron. **56**, 300–306 (2014)
35. Y. Zhang et al., Simultaneous voltammetric determination for DA, AA and NO2 – based on graphene/poly-cyclodextrin/MWCNTs nanocomposite platform. Biosens. Bioelectron. **26**, 3977–3980 (2011)
36. J. Wang et al., Rapid detection of nitrite based on nitrite-oxidizing bacteria biosensor and its application in surface water monitoring. Biosens. Bioelectron. **215**, 114573 (2022)
37. S. Palanisamy et al., A novel amperometric nitrite sensor based on screen printed carbon electrode modified with graphite/β-cyclodextrin composite. J. Electroanal. Chem. **760**, 97–104 (2016)
38. V. Sudha et al., Hierarchical porous carbon derived from waste Amla for the simultaneous electrochemical sensing of multiple biomolecules. Colloids Surf. B Biointerfaces **177**, 529–540 (2019)
39. S. Nasraoui et al., Electrochemical sensor for nitrite detection in water samples using flexible laser-induced graphene electrodes functionalized by CNT decorated by Au nanoparticles. J. Electroanal. Chem. **880**, 114893 (2021)
40. M.A. Zafar et al., Expeditious and eco-friendly fabrication of Graphene-Ag nanocomposite for Methyl Paraben sensing. Appl. Surf. Sci. **638**, 158006 (2023)

Authors and Affiliations

Scarlett Allende[1] · Yang Liu[2] · Muhammad Adeel Zafar[1] · Mohan V. Jacob[1]

✉ Mohan V. Jacob
Mohan.Jacob@jcu.edu.au

[1] Electronics Material Lab, College of Science and Engineering, James Cook University, Townsville, QLD 4811, Australia

[2] College of Science and Engineering, James Cook University, Townsville, QLD 4811, Australia